Eur. Phys. J. B (2012) 85: 50
DOI: 10.1140/epjb/e2011-20679-6

THE EUROPEAN PHYSICAL JOURNAL B

Regular Article

Traces of the evolution from Mott insulator to a band insulator in the pair excitation spectra

B.D. Napitu[1,2,a] and J. Berakdar[1,3]

[1] Institut für Physik, Martin-Luther-Universität Halle-Wittenberg, 06120 Halle, Germany
[2] Max-Planck-Institut für Mikrostrukturphysik, Weinberg 2, 06120 Halle, Germany
[3] School of Physics, The University of Western Australia, 35 Stirling Hwy, Crawley, WA 6009, Australia

Received 18 August 2011 / Received in final form 21 December 2011
Published online 8 February 2012 –

Abstract. We inspect the fundamental difference between the correlated band insulators (BI) and the Mott insulators (MI) from the perspective of the dynamical pair excitations. To this end, we investigated the physics of the two-plane Hubbard model by employing the well-tested dynamical mean field theory (DMFT) together with the quantum Monte Carlo (QMC) method. At half-filling our results clearly indicate that while the spectral weight of the pair excitation becomes minimal at MI which corresponds to a diminishing of the double occupancy, the opposite occurs at BI. We then discuss the effect of doping and find that the correlated band insulator and the Mott insulator robust at low doping concentration and the metallic state emerges at larger doping. The pair spectral function demonstrates that the metallic state of doped MI is strongly different from that of doped BI and it is readily reflected in the lineshape of the spectra. We discuss the implication of our results in the context of the two-particle spectroscopy.

1 Introduction

The transition from metallic to insulating phase is a ubiquitous phenomenon in solid state physics and has been one of the central research themes for more than four decades. A prototypical example is the Mott transition where the itinerant state transforms to a localized state whenever the magnitude of the local Coulomb interaction becomes large relative to the bandwidth. Materials of this class are referred to as strongly correlated electron systems. Well-studied cases are transition metal oxides such as $A_{1-x}B_xMO_3$: A=Sr, Ca, B=La,Y and M=Ti,V,Cr, where the degree of electronic correlations is known to be strongly dependent on the variation of the pressure or on the substitution of a specific element. In the last two decades, significant progress in the theoretical understanding of the Mott transition has been achieved thanks to the development of the dynamical mean field theory (DMFT) that connects the Brinkmann-Rice picture and the strong coupling Hubbard theory [1]. It is now established that the Mott metal insulator transition (MIT) is an example where the dynamical local fluctuations play a significant role and thus allows one to map the complex lattice problems onto the single-site action supplemented by the self-consistent equations.

For weakly correlated systems, the mechanism underlying MIT is different from that for strongly correlated electrons. The band insulating state can be described reasonably well within a picture based on an effective single-particle moving in the field of the ions. A prominent representative of these theoretical approaches is the density functional theory (DFT) within its local-density approximation. Nonetheless, these materials may show a variety of intriguing phenomena such as the quantum Hall effect, the Kondo insulator, and also the topological insulators see for e.g. references [2–6]. In the latter case, it becomes clear recently that the band insulating character of the bulk can coexist with a metallic states at the surface provided that there is a sufficiently large spin-orbit interaction. The question of whether such a property may be encountered also for strongly correlated systems is currently under discussion [7].

In recent years, there has been an upsurge of interest in studying the role of the electronic correlations in the band insulator and its connection to the Mott insulator (see e.g. Refs. [8,9]). In order to describe this novel property, one of the most extensively employed description is the ionic Hubbard model (IHM) that incorporates the local Coulomb interaction U and the one-body potential Δ [10–14]. The interplay of both parameters can lead to both the Mott insulator when $U > \Delta$ and the band insulator in the opposite case for $U < \Delta$. The rigorous analytical treatment of the 1D IHM suggested that BI and MI are separated by two continuous phase-transition; from BI to spontaneous-dimerised insulating (SDI) and followed

[a] e-mail: bnapitu@mpi-halle.mpg.de

by another transition to MI when the local interaction increases [15,16]. There have been many subsequent efforts to verify this proposal by performing the finite size numerical simulation. The results from the density matrix renormalization group (DMRG), the QMC, the exact diagonalization and the valence bonds technique have confirmed the existence of the intervening state at the moderate local interaction [17–23]. Conflicting results however exist particularly on the critical properties between BI and SDI and whether the MI state arises at pronounced U. The study of IHM at higher dimension has been also conducted recently on various levels of approximation. Both DMFT and quantum monte carlo clearly demonstrated the existence of the finite metallic region between the BI and the MI [24–27]. The cluster-DMFT and the variational cluster approximation on the other hand, predicted bond-ordered phase as an intermediate state and it was shown that there is a single metallic point at the phase boundary [28,29]. The precise phase diagram of IHM for one and for higher dimension thus remains an open question.

Besides IHM, another interesting system is the bilayer Hubbard model. Results from the DMFT-based approach have provided the evidence for the absence of any intervening phase between MI and BI and the two phases are suggested to be continuously connected [30–33]. The same, however, is not true for the two dimensional system studied within CDMFT and the determinant QMC [34,35]. It is shown that the metallic state becomes evident between BI and MI at weakly coupled layer, while direct crossover is observed when both layers are strongly coupled. The entrance of the metallic character at weak interplane hopping has been argued to be associated with the pronounced spatial fluctuation at low dimensional system which can not be captured in the traditional single-site DMFT. Whether this is a generic feature of the 2D-bilayer system, is presently not clear and remains to be elucidated.

While the discussion of the nature of the transition between BI and MI has been extensively performed in the last years, the question on how to address this issue experimentally has not been carefully considered. In the theoretical works, the most frequently used quantity to demonstrate the existence of BI/MI and the possible intermediate states is the single-particle or the particle-hole excitation (e.g. spin excitation, optical conductivity) which in general can be verified experimentally. In the former case, the calculated single-particle spectral function is known to be related directly to the spectra of the angular-resolved photoemission spectroscopy (ARPES) [36]. Definitive experimental evidence for the evolution of MI to BI is, to our knowledge, not yet available on the basis of this approach. It is therefore of interest to explore an alternative experimental technique that is capable of assessing the underlying physics of correlated BI and MI. One possible proposal in this connection, is to employ the two-particle spectroscopy which in recent years have seen a rapid development in its energy resolution allowing to inspect the electronic properties of solids [37,38]. Experimentally, this method is known as the $(\gamma, 2e)$ spectroscopy where a pair of indistinguishable particles is ejected upon the absorption of a VUV photon [39,40]. This approach is the extension of ARPES and can be employed to produce the spectral properties of the valence band. One of the most crucial aspect of this technique is that both particles have to be detected coincidentally to ensure that the excited particles come from the same scattering event [37,39–41]. Theoretically, it is shown that this condition can be fulfilled only if the ejected particles are initially correlated [42]. In the past, there are a number of studies in the literature that document the application of this technique on the simple metal, semiconductor and disorder system [43–46]. On the other hand, the investigation of the properties of the strongly correlated electrons within $(\gamma, 2e)$ spectroscopy has not received considerable attention and the research on this issue has begun only recently in theoretical study of the single- and the two-band Hubbard model [47]. On the basis of DMFT, it was argued that the pair of electrons is useful to explore the physics of strongly correlated material particularly in the vicinity of the Mott transition. The application of this experimental technique to elucidate the physics of MI that is linked to the BI, therefore constitutes a challenging task which is expected to provide new insights beyond the single-particle level.

Our aim in the present work is to inspect the correlated band insulator and the Mott insulator from the perspective of the particle-particle excitation/pair excitation that is relevant to the $(\gamma, 2e)$ spectroscopy. To this end, we study the bilayer Hubbard model in the framework of the DMFT and the quantum Monte Carlo (QMC) method. The results are presented at both half-filling and upon doping the BI and the MI. The organization of the paper is as follows. We present in the next section the reference model and the method of solution. This is then followed by the presentation of the main results started at half-filling and then doped insulating state. The last section contains concluding remarks.

2 Model and theoretical methods

The Hamiltonian of the two-plane Hubbard model in the second quantization reads

$$H = -t \sum_{ij\alpha\sigma} c^{\dagger}_{i\alpha\sigma} c_{j\alpha\sigma} - t' \sum_{i\alpha\sigma} c^{\dagger}_{i\alpha\sigma} c_{i,1-\alpha\sigma} + U \sum_{i\alpha} n_{i\alpha\uparrow} n_{i\alpha\downarrow} \tag{1}$$

where t, t' denote the intra- and the inter-layer hopping amplitudes while U is the on-site Coulomb interaction. In the above notation, α and σ index the planes and spins respectively. The DMFT can then be straightforwardly applied to the Hamiltonian of equation (1), by noting that each plane is mapped onto a single site while the rest of the sites is subsumed into a Weiss field. The full-interacting Green's function in the Matsubara representation $\mathcal{G}(i\omega_n)$ can be expressed as follows

$$\mathcal{G}(i\omega_n) = \sum_{\mathbf{k}} \frac{1}{(i\omega_n + \mu)\mathcal{I} - \mathcal{H}(\mathbf{k}) - \Sigma(i\omega_n)}. \tag{2}$$

Here, $\mathcal{G}$ is a 2×2 matrix of Green's function defined on the discrete set of Matsubara frequencies $\omega_n = (2n+1)\pi$T, and $\mathcal{I}$ denotes the corresponding identity matrix. The relation between the interacting Green's function and the Weiss field $\mathcal{G}_o(i\omega_n)$ is provided by the Dyson equation using the self energy $\Sigma(i\omega_n)$, i.e.

$$\mathcal{G}^{-1}(i\omega_n) = \mathcal{G}_o^{-1}(i\omega_n) - \Sigma(i\omega_n). \quad (3)$$

In the DMFT, the information of the lattice enters through $\mathcal{H}(k)$ that consists of diagonal elements for the in-plane dynamics and off-diagonal for the inter-plane hopping t'

$$\mathcal{H}(\mathbf{k}) = \begin{pmatrix} \epsilon(\mathbf{k}) & t' \\ t' & \epsilon(\mathbf{k}) \end{pmatrix}. \quad (4)$$

This matrix can be easily diagonalized following the symmetry consideration such that the full interacting Green's function of equation (2) can be written in terms of bonding and antibonding representation. The solution of the local action of the Hamiltonian of equation (1) is then obtained via Hirsch-Fye QMC by which the Green's function for the single- and the two-particle can be derived [48]. This approach is complemented by the maximum entropy method (MEM) to obtain the real-frequency axis of the single- and the two-particle spectral function [49].

For the purpose of deriving the particle-particle or doublon spectral function, we consider in what follows the two-particle Green's function

$$\chi_{pp}^{(\sigma,\sigma')}(\mathbf{q}, i\omega_m) = \int \langle T_\tau c_{\mathbf{k},\sigma'}(\tau) c_{\mathbf{q}-\mathbf{k},\sigma}(\tau) c^\dagger_{\mathbf{q}-\mathbf{p},\sigma}(0) c^\dagger_{\mathbf{p},\sigma'}(0)\rangle. \quad (5)$$

Here, $\int$ is a short-hand notation for $-\sum_{\mathbf{kp},\sigma}\int_0^\beta d\tau e^{i\omega_m\tau}$ and $\omega_m = \frac{2m\pi}{\beta}$ corresponds to the Matsubara frequency. In addition, T_τ is an ordering operator for τ. The two-particle propagator will be evaluated within two different schemes namely within DMFT + QMC loop and with the perturbation theory utilizing the ladder diagrams. In the former case, DMFT + QMC provides the local version of the particle-particle propagator reads

$$\chi_{pp}(\tau) = \left\langle T_\tau \Delta^\dagger(\tau)\Delta(0)\right\rangle, \quad (6)$$

with $\Delta = c_\uparrow c_\downarrow$.

Within perturbation theory , the summation of ladder diagrams leads to [47]

$$\chi_{pp}(\mathbf{q}, i\omega_m) = \frac{\chi(\mathbf{q}, i\omega_m)}{1 - U\chi(\mathbf{q}, i\omega_m)} \quad (7)$$

where

$$\chi(\mathbf{q}, i\omega_m) = -\frac{1}{\beta}\sum_{\mathbf{p}, i\nu_n} \mathcal{G}(\mathbf{p}, i\nu_n)\mathcal{G}(\mathbf{q}-\mathbf{p}, i\omega_m - i\nu_n) \quad (8)$$

is the two-particle Green's function expressed in terms of the fully interacting single-particle Green's function. Note that in the above equation, ν_n (ω_m) and β correspond to the Matsubara frequencies of fermions (bosons) and the inverse temperature, respectively.

The dynamical properties of two-particle propagator are then readily obtained from the imaginary part of $\chi_{pp}(\tau)$:

$$P(\omega) = \mathrm{Im}[\chi_{pp}(\mathbf{q}, \omega + i\delta)]. \quad (9)$$

As mentioned above, within the DMFT + QMC scheme this last step is performed via MEM by using the bosonic kernel [49]. On the other hand, the evaluation of equation (7) can be done efficiently in terms of the single-particle spectral function which will be provided by DMFT results. In this respect, it is sufficient to express equation (8) on the real axis representation as follows

$$\chi_i(\omega) = \mathscr{C}_0 \int_{-\infty}^{\infty} d\nu \int_{-\infty}^{\infty} d\epsilon D(\epsilon)\,[A(\epsilon,\nu)A(-\epsilon,\omega-\nu) \times (1 - f(\nu) - f(\omega-\nu)] \quad (10)$$

where $\chi_i(\omega)$ stands for the imaginary part of $\chi(i\omega_m)$, $f(\omega)$ is the Fermi distribution function and $A(\epsilon,\omega) = -\frac{1}{\pi}\mathrm{Im}\left[\frac{1}{\omega-\epsilon-\Sigma(\omega)}\right]$ is the full interacting single-particle spectral function. $D(\epsilon)$ is the free density of states while $\mathscr{C}_0$ denotes the additional constant. The real part of equation (10) is readily obtained from the Kramers-Kronig relation following the causality principle.

The dynamical properties of the two-particle excitations are constrained by the sum rule

$$\int P(\omega)d\omega = d \quad (11)$$

where $d = \langle n_\uparrow n_\downarrow\rangle$ corresponds to the double occupancy evaluated directly within DMFT + QMC. A very useful quantity to check the consistency of the spectra is the dynamical counterpart of equation (11), $K_p(\Omega)$, reads

$$K_p(\Omega) = \int_0^\Omega P(\omega)d(\omega). \quad (12)$$

In what follows, we present the results of the two-plane Hubbard model in the paramagnetic phase by employing the Bethe lattice density of states (DOS) which represents the bare in-plane structure. Unless otherwise stated, the bandwidth $W = 1$ is set as the unit energy and the temperature is $T/W = 0.0625$.

3 Results and discussion

3.1 Half-filling

Before discussing the results of the two-particle excitation, it is necessary to recall briefly the scenario for the crossover from the Mott insulator to the correlated band insulator from the perspective of the single-particle spectral function as sketched in Figure 1. The presented results corresponds to the imaginary part of the single-particle Green's function of both planes which are calculated at half-filling, namely that the occupation of each plane is

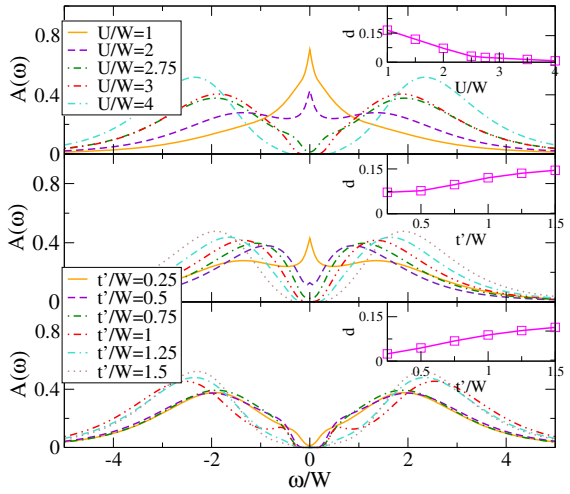

Fig. 1. (Color online) The single-particle spectral function of the two-plane Hubbard model at half-filling as a function of the Coulomb interaction but for fixed inter-plane hopping $t'/W = 0.25$ (top panel). The results upon varying the inter-plane hopping at constant Coulomb interaction are shown in the middle ($U/W = 2$) and in the lower ($U/W = 2.75$) panel. Here, the single-particle energy ω is measured relative to the bandwidth W. The inset on each panel indicates the magnitude of the double occupancy d as a function of the Coulomb interaction (top panel, $1 \leq U/W \leq 4$) and as a function of the inter-plane amplitude (middle and lower panels, $0.25 \leq t'/W \leq 1.5$).

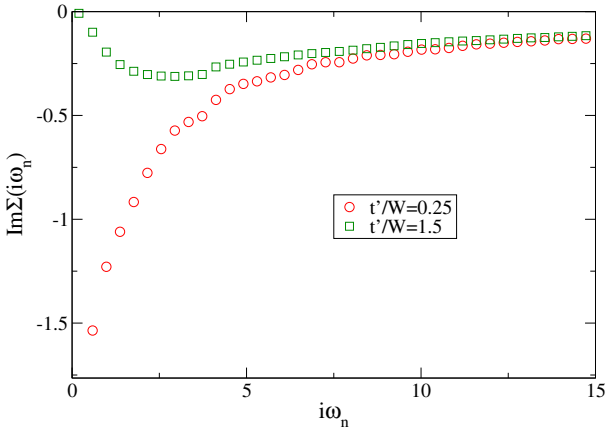

Fig. 2. (Color online) The imaginary part of the single-particle self-energy ImΣ on the Matsubara axis $i\omega_n$ at $U/W = 2.75$ calculated under the same condition as in Figure 1. Here, the inter-plane coupling $t'/W = 0.25$ corresponds to the Mott insulator while $t'/W = 1.5$ denotes the band insulator.

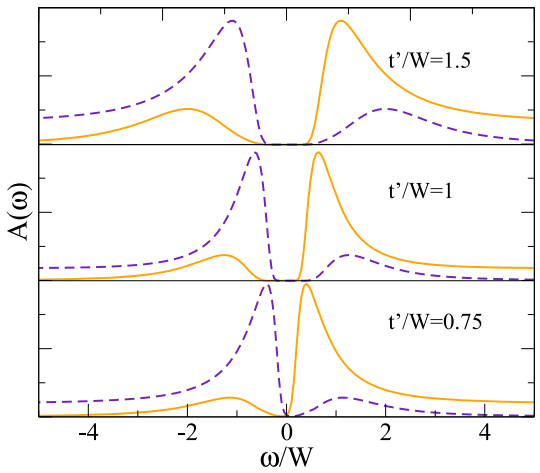

Fig. 3. (Color online) The same as in Figure 1. In the present case however, we show the evolution of the single-particle spectra in the anti-bonding (solid lines) and the bonding bands (dashed lines) representation for various t'/W and at $U/W = 2$.

equal $\tilde{n}_1 = \tilde{n}_2 = 1$ and the average occupation n satisfies the condition $n = \frac{1}{N}\sum_\alpha \tilde{n}_\alpha = 1$ (N denotes the number of the plane). At constant inter-plane hopping $t'/W = 0.25$ but for various values of the Coulomb interaction (see top panel), the spectra of the two-plane Hubbard model clearly suggest a Mott metal insulator transition. The quasiparticle peak at a weak coupling, the hallmark of the Fermi liquid character collapses as a function of the on-site interaction and the gap is formed at the Fermi level when U/W is pronounced. In addition, one observes that the double occupancy $d = \langle n_\uparrow n_\downarrow \rangle$ (inset of the top panel of Fig. 1) diminishes as a function of U/W and the self energy (see Fig. 2 for $t'/W = 0.25$) diverges as the system enters the Mott insulating phase [1].

The gap opening which marks the insulating state can be also realized by varying the inter-plane coupling t'/W as shown in the middle and the lower panel of Figure 1. At $U/W = 2$, the destruction of the quasiparticle peak is readily observed upon the increase of the inter-layer coupling which is then followed by the formation of the gap beyond $t'/W = 0.75$. The somewhat similar situation is also noticeable at $U/W = 2.75$, the onset of the Mott insulating state. The enhancement of the inter-plane coupling leads to the broadening of the gap and implies an increase of the insulating behavior. Having examined the character of the double occupancy (middle and bottom panel of Fig. 1) and the self energy (see Fig. 2 at $t'/W = 1.5$), it becomes clear that the underlying mechanism behind the gap opening in the present case is different from those generated by U/W. This is hinted at by the positive slope of d with maximum value at $t'/W = 1.5$. In the self-energy data, it is shown that at pronounced inter-plane hopping the low energy part extrapolates to zero with a considerably large spectral weight; an opposite character to the one observed in the Mott insulator.

In order to understand the origin of the gap at enhanced t'/W, it is important to note that the bonding and the antibonding bands become evident upon the collapse of the quasiparticle peak. Examples of this representation are shown in Figure 3 at $U/W = 2$ where the bonding/antibonding character becomes more and more visible at higher t'/W which is also accompanied by a large splitting. We can therefore deduce that the gap at pronounced t'/W is a direct consequence of the complete separation of the bonding and the antibonding bands and signal for the emergence of the band insulating (BI) character. Now,

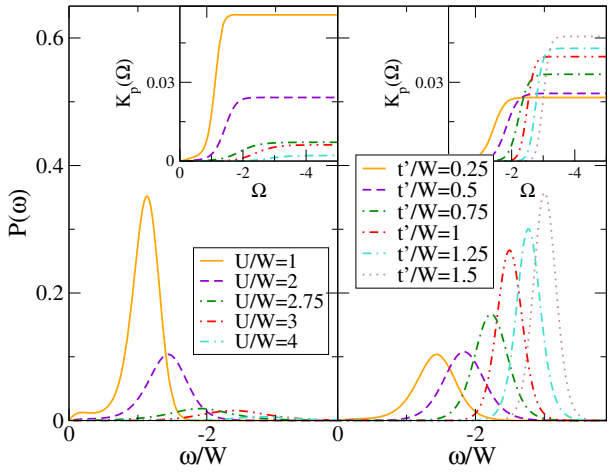

Fig. 4. (Color online)The frequency dependence of the two-particle spectral function at half-filling. Various curves on the left panel correspond to different values of the on-site Coulomb interaction U/W at fixed $t'/W = 0.25$, whereas the right panel explore the effect of the inter-plane-hopping amplitude at $U/W = 2$. Here ω corresponds to the shared energy between the two electrons relative to W. Insets show the integrated spectral function, calculated according to equation (12).

since the BI, upon varying the inter-plane hopping, occurs not only in the regime of weakly interacting but also at higher U/W (see e.g. $U/W = 2.75$), one can directly infer that there is a direct crossover from MI to BI. Our DMFT results for the dynamical single-particle properties presented above support the previous findings within the DMFT scheme that also indicate the absence of the intermediate states between BI and MI [30–32].

Armed with the knowledge of the nature of crossover from BI to MI in the bilayer Hubbard model, let us now discuss the same issue via the lineshape of the pair excitation. As is already pointed out earlier, we performed two different formalisms in this respect on the basis of the self-consistent DMFT loop and the combination of the DMFT and the ladder approximation. We first consider in what follows the results obtained in the former case as depicted in Figure 4. Here ω corresponds to the shared energy of the pair of electrons. The evolution of the pair spectral function upon varying the Coulomb interaction is displayed on the left panel of Figure 4 obtained with a constant inter-plane hopping $t'/W = 0.25$. For weakly interacting systems, the spectral function is characterized by an intense peak and finite low-energy. Upon the increase of electronic interaction, the spectral weight decays and the peak shifts to higher energies (away from $\omega = 0$). The same trend is evident when U/W further increases in such a way that there is a formation of gap with only small spectral weight in the Mott insulating regime, $U/W \geq 2.75$. The meaning of this results is more readily apparent from the integrated spectra, $K_p(\Omega)$, which is plotted in the inset of the left panel of Figure 4. Here, the spectral weight of $K_p(\Omega)$ also diminishes as a function of U/W and resembles the behavior of $P(\omega)$. By using the relation expressed in equation (11) that links the integrated spectra and the double occupancy, the suppression of $K_p(\Omega)$ amounts to saying that the double occupancy becomes less probable as the electronic correlation increases which is indeed expected in the Mott transition. The reduction of the spectral weight together with the formation of the low energy gap both at $P(\omega)$ and at $K_p(\omega)$ is an unequivocal signal for the transition from a metallic Fermi-liquid onto a Mott insulating phase and is considered as a remarkable feature of the pair spectral function [47]. The essential ingredient that drives the emergence of the Mott insulator is directly embodied in the lineshape of the spectra and the whole trends mimic that observed in the double occupancy data depicted in the inset of the top panel of Figure 1.

Next, we vary the inter-plane hopping while maintaining the magnitude of the Coulomb interaction. The results for $U/W = 2$ are depicted in the right panel of Figure 4. At weakly coupled plane $t'/W = 0.25$, the spectral function is characterized by broad response with finite low energy that signifies the metallic character. As inter-plane hopping becomes stronger, the resonance shifts to upper energies which is also accompanied by the increase of the spectral weight. The same trend is evident when the coupling between the planes is enhanced up to t'/W=1.5 where one observes sharp-peaked spectra with the largest low energy gap. The weight of the integrated spectra $K_p(\Omega)$ as a function of the inter-plane hopping (inset of the right panel of Fig. 4) also indicates the same trend. On the basis of the sum-rule relation of equation (12), we can conclude that for strongly coupled plane there is an increase of the probability of the double occupancy. We have seen above using the static double occupancy that this behavior is understood as a signal for the emergence of the band insulator.

In order to understand the reason why the pair spectra as a function t'/W exhibit such a behavior, one recalls the fact that BI is characterized by either empty or fully occupied bands. In the present context, this is manifested in the formation of a more double occupancies and/or empty states. Since this quantity is closely related to the spectral weight of the particle-particle spectra (see Eq. (12)), the increase of double occupancy amounts to enhancing the weight of the pair spectral function. It is interesting to note that the rise of double occupancy also explains the reason for the formation of a low energy gap in the local spin susceptibility or equivalently for the diminishing of the local moment in the BI regime. The enhancement of the onsite pairs at the strongly coupled plane suppresses the onsite fluctuations which in turn inhibits the formation of the paramagnon peak at the spin susceptibility [30,32] .

In order to observe the continuous transition from MI to BI in the pair spectral function we plot the calculated spectra at $U/W = 2.75$ (left panel of Fig. 5). It can be directly deduced that the MI state at $t'/W = 0.25$ can evolve smoothly to the BI state at $t'/W = 1.5$. The spectral weight of $P(\omega)$ as well as the integrated spectra increases gradually as a function of t'/W and becomes maximum at strong inter-plane coupling. The pair spectral function therefore provides support for the notion of direct crossover from MI to BI which is in a good agreement with

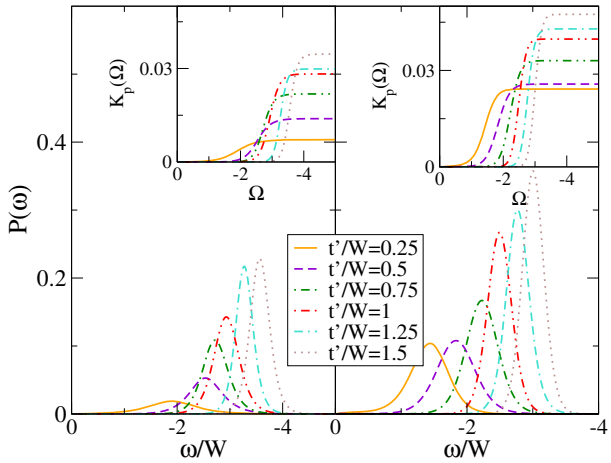

Fig. 5. (Color online) The same as in Figure 4 for various values of the inter-plane coupling. The left panel corresponds to $U/W = 2.75$ at $T/W = 0.0625$ (as in the previous figures) while the results in the right panel are obtained at lower temperature $T/W = 0.03125$ and by setting the Coulomb interaction at $U/W = 2$.

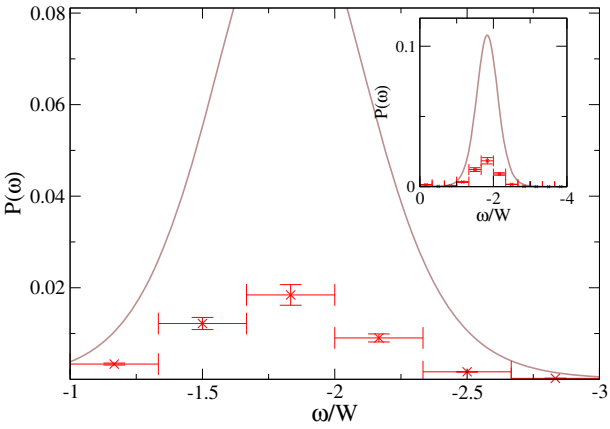

Fig. 6. (Color online) P(ω) obtained within the same condition as in Figure 4 for $U/W = 2$ and $t'/W = 0.5$. The x-points correspond to the integrated spectral function within 12 non-overlapping regions of width indicated by the horizontal error-bar. The uncertainty of the integrated weight is denoted by the vertical error-bar. Inset shows the full scale.

the single-particle spectral function. We note in passing that the character of BI and MI persists at lower temperature. As an example, we show the two-particle spectral function at lower temperature $T/W = 0.03125$ for various values of inter-plane hopping, at $U/W = 2$ (right panel of Fig. 5). The evolution of the lineshape of $P(\omega)$ from weak to stronger t'/W is relatively comparable to that in the right panel of Figure 4 and BI at large inter-plane coupling is evidenced by the wide gap and the pronounced spectral weight.

Before discussing the results of the ladder approximation, a few remarks should be made on the quality of the two-particle spectra presented above. Figure 6 depicts the results of the pair spectral function at $U/W = 2$ and $t'/W = 0.5$ together with the error estimates. We note

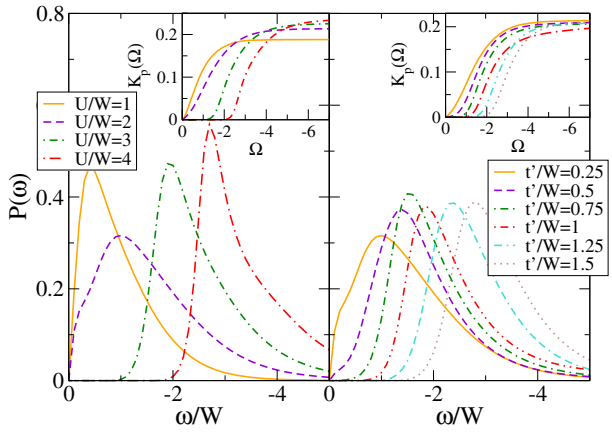

Fig. 7. (Color online) The spectral function of the two-particle excitations from the ladder approximation. The results are obtained by using the same parameters set for Figure 4.

that errors on each point can not be evaluated due to the fact that they are strongly correlated between different points and also since the spectral function corresponds to the probability on certain region [49]. What is shown here is therefore the integrated spectral density on 12 non-overlapping regions with its error bar. From the figure, it can be concluded that MEM delivers precise spectral function for two-particle as indicated by the small uncertainty of the integrated spectra.

In the next paragraphs, we discuss the pair spectral function derived from the ladder approximation. The results are plotted in Figure 7. In the left panel, we show the pair spectra upon the variation of the Coulomb interaction under the same condition applied in Figure 4. At weakly coupled plane, the spectral function lies close to $\omega/W = 0$ which signifies the metallic character. The increase of interaction amounts to shifting the spectral function onto upper energies which eventually leads to the opening of the gap. The emergence of the gap can be seen as direct consequence of the convolution in equation (10) and is associated with those observed in the single-particle spectral function. The ladder approximation, however, does not deliver a reasonable spectral weight dependency which eventually violates the two-particle sum rule. The increase of $K_p(\Omega)$ (inset of Fig. 7) which implies the enhancement of double occupancy, is in contrast to the fact expected for the Mott transition.

The same is apparently true for the results upon varying t'/W at $U/W = 2$ as sketched in the right panel of Figure 7. The ladder approximation delivers accurate description only on the gap opening while it misses the change of the spectral weight when the inter-layer coupling increases. In order to understand the origin of this inconsistency, one recalls the fact that the single and the doublon are not calculated on an equal level of approximation and the self consistency is performed only on the single-particle level. Both aspects are however necessary to ensure that the correlation on the single-particle level will be also recorded in the two-particle, and vice-versa [47]. We argue that this is fulfilled by the first scheme in which

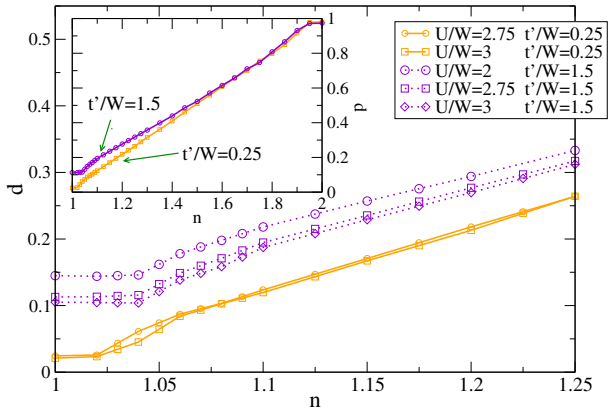

Fig. 8. (Color online) Double occupancy d as a function of the occupation number n for various values of t'/W and U/W. In the main panel, the effect of doping for MI and BI are shown in the range of $1 \leq n \leq 1.25$ where the former is indicated by the solid lines while the latter by the dashed lines. The same is also shown in the inset. Here, the results are obtained for all possible ranges of doping at $U/W = 2.75$. Note that the lines are the guide to the eyes.

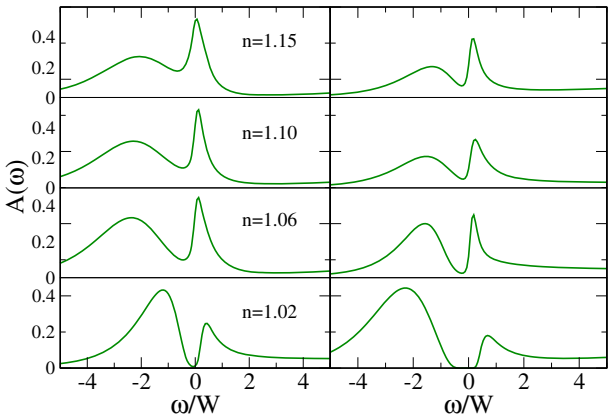

Fig. 9. (Color online) The single-particle spectral function of the doped Mott insulator (left panel) and the doped correlated band insulator (right panel) for a different number of the occupation n. The results are obtained at $U/W = 2.75$ where the inter-plane coupling of doped MI and doped BI are set to $t'/W = 0.25$ and $t'/W = 1.5$ respectively.

the two-particle correlation function is obtained directly within DMFT loop.

3.2 Effect of doping

Let us now consider the effect of doping on the bilayer Hubbard model by adding the hole/particle on the Mott and the band insulator. As before, both layers are set to have an equal occupation number meaning that the doping is considered to be distributed uniformly. We note also that, albeit away from half-filling our DMFT + QMC calculations did not indicate any sign problems for all ranges of doping. In what follows, we first examine the double occupancy d as a function of the average occupation number n for various strengths of the Coulomb interaction and the inter-plane hopping as depicted in Figure 8. Here, the Mott and the band insulator at half filling are distinguished by the inter-layer hopping at $t'/W = 0.25$ and at $t'/W = 1.5$ respectively. At low doping concentration, for $n \leq 1.05$, one readily sees that the double occupancy remains pinned to the same value of the insulating state which reflects the persistence of MI and BI. The doped MI is shown to be quantitatively smaller than that of BI owing to the fact that there is a pronounced correlation at MI regime that hinders the formation of the double occupancy. Beyond $n \approx 1.05$, the double occupancy gradually shows linear dependency on n with positive slope which becomes more tangible as n goes away from half-filling. This can be taken as a signal for the emergence of the metallic behavior following the facts that the additional particles have occupied the sites of the lattice and consequently suppress the correlation. The fact that the doped MI quantitatively smaller than that of doped BI is a signal that the correlation of the former remains stronger than that the latter. The emergence of this behavior can be understood by recalling that there is a continuous transition from the insulating to the metallic state in such a way that the nature of correlation of BI or MI persists over a wide range of doping. As the occupation number increases $n > 1.5$, the effect of correlation diminishes which is reflected in the overlapping of the doped BI and the doped MI (see inset of Fig. 8).

The enhancement of metallic character upon doping of MI and BI is also detectable in the lineshape of the single-particle spectral function. The results are shown in Figure 9 as a function of the occupation number n. It can be immediately recognized that at low doping concentration $n = 1.02$, the spectral function of both doped MI and doped BI consists of gap which signals the persistence of the insulating character. When n increases, the metallic behavior becomes more and more noticeable as demonstrated by the emergence of the quasiparticle peak and simultaneously by the degradation of the pseudo-gapped feature. We note here that the doped BI and the doped MI remain distinguishable for all calculated doping which reflects the different nature of the correlation. In order to address precisely the underlying physics behind these metallic behavior, it is instructive to examine the imaginary part of the self energy which is plotted in Figure 10.

The low energy part of the doped BI obviously differs from that of the doped MI. In the former case, one directly observes a linear behavior at low frequencies which can be extrapolated to zero. The metallic state upon doping BI therefore corresponds to a good metallic behavior with well-defined quasiparticle. In contrast, the self-energy of the doped Mott insulator at $t'/W = 0.25$ indicates finite value at $i\omega \to 0$. This is clearly a signal for a metallic system that violates the Fermi liquid character. The emergence of two metallic character at high doping concentration is thus evident which is related to the strength of the electronic correlation.

To further substantiate our arguments, we supplement the above results with the dynamical properties of the two-particle excitation. We first examine the imaginary

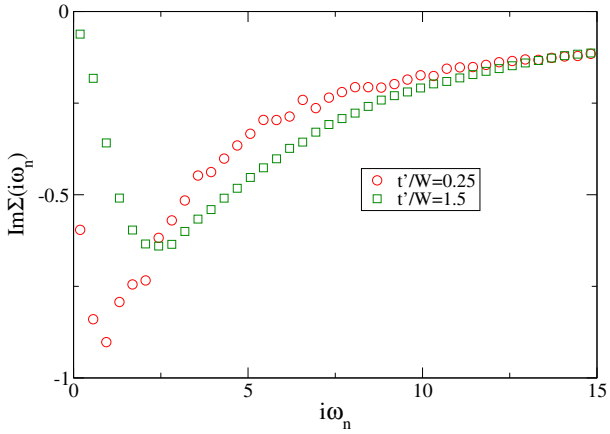

Fig. 10. (Color online) The imaginary part of the self energy on the Matsubara axis $i\omega$ for $n = 1.10$ at fixed $U/W = 2.75$. The same as in Figure 9, the Mott and the band insulator upon doping are identified from the magnitude of the inter-plane hopping t'/W at 0.25 and at 1.5 respectively.

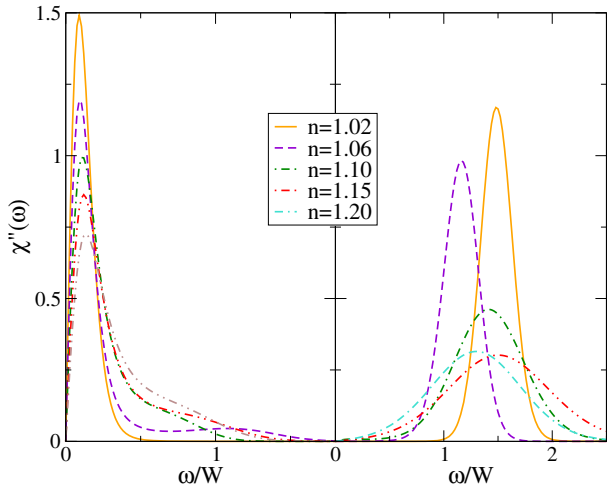

Fig. 11. (Color online) The dynamical spin susceptibility $\chi''(\omega)$ of the two-plane Hubbard model away from half-filling. The doped MI corresponds to $t'/W = 0.25$ (left panel) while the doped BI is obtained at $t'/W = 1.5$ (right panel). The Coulomb interaction is maintained at $U/W = 2.75$.

part of the dynamical spin susceptibility $\chi''(\omega)$ of doped MI and doped BI in the left and in the right panels of Figure 11 respectively. We note that the results are calculated under the same parameter range as in Figure 9 and they are derived from the spin-spin correlation function $\chi(\tau) = \langle T_\tau S_z(\tau) S_z(0)\rangle$. The different nature of the doped BI and the doped MI is readily observed at low doping and even more so for the overdoped case. One of the most conspicuous feature is the resonance peak which is found to occur dominantly at low energy (near $\omega \to 0$) for doped MI and at high energy for doped BI (note also the gap at low energy). The former is a well-known low-energy excitations that reflect the pronounced correlation at the verge of the Mott insulator regime while the latter is the signature of the suppression of local moment in the band

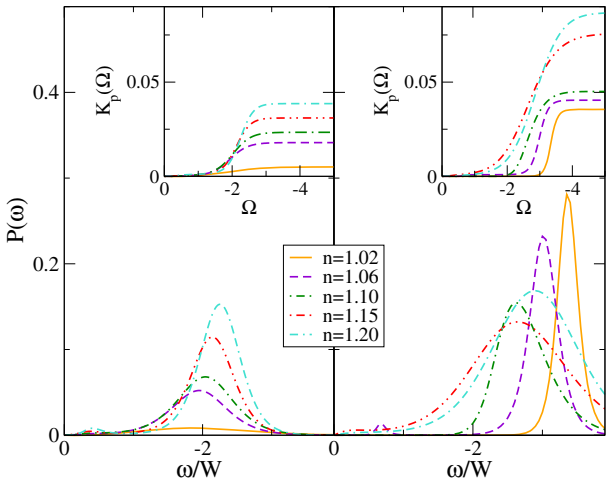

Fig. 12. (Color online) The pair spectral function $P(\omega)$ as a function of the total occupation number n at fixed $U/W = 2.75$. While the left panel indicates the evolution of the spectral function upon doping the Mott insulating state at $t'/W = 0.25$, the right panel displays the results of the correlated band insulating state at $t'/W = 1.5$. Insets depict the integrated spectral function $K_p(\Omega)$.

insulating phase as we already pointed out above. The spectral weight of the spin susceptibility then decreases as the doping is further enhanced. For doped BI, it can be seen that in addition to this, the spin gap becomes less pronounced and completely disappears at large doping. It is remarkable to note that the low-energy resonance of doped MI remains substantial up to $n = 1.20$, while the resonance of doped BI for $n \geq 1.10$ always lies at higher energies. The emergence of this character is strongly related to the nature of correlation in the doped BI and the doped MI which also explains the reason behind the separation of metallic state up to $n \approx 1.50$.

In order to elaborate on the above results, we discuss in what follows the pair spectral function upon doping the insulating state under the same condition as in Figure 11. The results are depicted in Figure 12 where the left and the right panels denote the results for the doped MI and the doped BI respectively. The persistence of the insulating character is directly noticed upon examining the weight and the existence of the gap in the spectral function for $n = 1.02$. Here, the doped MI is characterized by the smallest spectral weight with considerably wide gap while doped BI is noted by an enhanced peak at higher energies. As doping increases, the adjustment of the lineshape of the pair spectra is evident where for doped MI, one observes the gradual enhancement of the weight and eventually reaches maximum in the overdoped regime at $n = 1.20$. The result of the integrated spectral weight $K_p(\Omega)$ resembles this behavior (see the inset of Fig. 12). The enhancement of $K_p(\Omega)$ clearly implies for the increase of double occupancy which is induced by the addition of particles/holes. The results of integrated spectra are therefore corroborate with the static properties of Figure 8. It is interesting that the spectral weight of BI

for all doping concentration is quantitatively larger than that of MI which implies that the formation of double occupancy in the latter case is less probable. This can be understood by recalling the fact that the local correlations remain pronounced at doped MI and the formation of double occupancy requires larger energy to overcome the local Coulomb barrier. The two-particle spectral function therefore provides another evidence for the different nature of the metallic character upon doping BI and MI below $n = 1.50$ which can be directly deduced from its spectral weight.

Before closing this section, let us now comment on whether or not the pair spectral function offers a reasonable route to assess the crossover from BI to MI. As is already seen, the effects induced by the local correlation, the inter-plane hopping and the doping are well-captured in the pair spectral function. At half-filling, the transition from metallic to BI, metallic to MI and from BI to MI are also realized in the spectral function of the doublon. Beyond this, it has been shown above that the pair excitation offers a straightforward way for identifying the emergence of the MI and the correlated BI as compared to the single-particle spectra. MI is characterized by a reduction of the spectral weight while the opposite is true for BI. In addition, the pair spectral function also provides direct information behind the underlying mechanism of BI and MI which is based on the probability of double occupancy. The inherent properties of the two-particle excitation are therefore, in general, useful to determine whether the transition belongs to the Mott type or to the other one.

We argue that the results presented above can be verified experimentally by means of the two-particle spectroscopy under the condition that the angles of the ejected particles and their energies are kept constant while the photon energy is varied [47]. This is necessary in order to obtain direct relation between the pair excitation $P(\omega)$ and the measured intensity in $(\gamma, 2e)$ spectroscopy. On the basis of the above observation, one can expect that the probability to eject a pair of particles will be higher in the correlated band insulator phase than that in the Mott insulator.

4 Conclusion

In summary, we have described theoretically the physics of BI and MI from the perspective of the two-particle spectral function that is related to the $(\gamma, 2e)$ spectroscopy. We solved the dynamical mean field theory equations for the two-plane Hubbard model at finite temperature by means of the quantum monte carlo method. At half-filling, we first explored the single-particle spectral function that exhibits a continuous crossover from the Mott insulating to the correlated band insulating phase, in line with previous studies. We then calculated the main quantity of interest, the pair spectral function that provides not only the evidence for the absence of the intervening states between BI and MI but also the underlying mechanism behind the emergence of both phases. At the vicinity of MI, the weight of the pair spectral function is strongly decreased as a function of local interaction which reflects the diminishing of the double occupancy or equivalently the suppression of the local charge fluctuation. The opposite is true for the correlated band insulating phase.

Away from half-filling, the correlated BI and the MI phases are found to persist at low doping concentration. The metallic behavior then gradually emerges as doping increases. It is shown that, while the doped MI and the doped BI remain distinguishable up to $n \approx 1.5$ they become comparable at considerably large doping. The nature of the metallic state for doped MI and for doped BI is discussed in detail on the basis of the results of the self-energy, the spin susceptibility and the pair spectral function. The dynamical spin susceptibility shows that the discrepancy between doped MI and doped BI is related to the behavior of the low-energy spin fluctuations which reflects the different strength of the correlation. In the pair spectral function, it is further shown that it is the probability of the formation of the double occupancy that strongly influences the metallic behavior of doped MI and doped BI.

This work is supported by the DFG through SFB 762. We thank Prof. Kirschner and F. Schumann for discussions on the $(\gamma, 2e)$ spectroscopy.

References

1. A. Georges, G. Kotliar, M. Rozenberg, W. Krauth, Rev. Mod. Phys. **68** 13, (1996) and references therein
2. V. Jaccarino, G. Wertheim, J. Wernick, L.R. Walker, S. Arajs, Phys. Rev. **160**, 476 (1967)
3. Z. Schlesinger, Z. Fisk, H.-T. Zhang, M. Maple, J.F. DiTusa, G. Aeppli, Phys. Rev. Lett. **71**, 1748 (1993)
4. K. Klitzing, G. Dorda, M. Pepper, Phys. Rev. Lett. **45**, 494 (1980)
5. X.L. Qi, S.C. Zhang, Phys. Today **63**, 33 (2010)
6. C. Petrovic, Y. Lee, T. Vogt, N. Lazarov, S. Bud'ko, P.C. Canfield, Phys. Rev. B **72**, 045103 (2005)
7. S. Raghu, X.L. Qi, C. Honerkamp, S.C. Zhang, Phys. Rev. Lett. **100**, 156401 (2008)
8. K. Tókar, P. Piekarz, M. Derzsi, P.T. Jochym, J. Lazewski, M. Sternik, A.M. Oles, K. Parlinski, Phys. Rev. B **82**, 195116 (2010)
9. A.F. Ho, Phys. Rev. A **73**, R061601 (2006)
10. J. Hubbard, J. Torrance, Phys. Rev. Lett. **47**, 1750 (1981)
11. N. Nagaosa, J. Takimoto, J. Phys. Soc. Jpn **55**, 2735 (1986)
12. T. Egami, S. Ishihara, M. Tachiki, Science **261**, 1307 (1993)
13. S. Ishihara, T. Egami, M. Tachiki, Phys. Rev. B **49**, 8944 (1994)
14. R. Resta, S. Sorella, Phys. Rev. Lett. **74**, 4738 (1995)
15. M. Fabrizio, A.O. Gogolin, A.A. Nersesyan, Phys. Rev. Lett. **33**, 2014 (1999)
16. C. Batista, A. Aligia, Phys. Rev. Lett. **92**, 246405 (2004)
17. L. Tincani, R. Noack, D. Baeriswyl, Phys. Rev. B **79**, 165109 (2009)

18. J. Lou, S. Qin, T. Xiang, C. Chen, G. Tian, Z. Su, Phys. Rev. B **68**, 045110 (2003)
19. S. Manmana, V. Meden, R. Noack, K. Schönhammer, Phys. Rev. B **70**, 155115 (2004)
20. T. Wilkens, R. Martin, Phys. Rev. B **63**, 235108 (2001)
21. M. Torio, A. Aligia, H. Ceccatto, Phys. Rev. B **64**, 121105 (2001)
22. N. Gidopoulos, N. Sorella, E. Tosatti, Eur. Phys. J. B **14**, 217 (2000)
23. A. Kampf, M. Sekania, G. Japaradize, P. Brune, J. Phys.: Condens. Matter **15**, 5895 (2003)
24. A. Garg, H.R. Krishnamurthy, M. Rahendra, Phys. Rev. Lett. **97**, 046403 (2006)
25. N. Paris, K. Bouadim, F. Herbert, G. Batrouni, R. Scalettar, Phys. Rev. Lett. **98**, 046403 (2007)
26. L. Craco, P. Lombardo, R. Hayn, G. Japaridze, E. Hartmann, Phys. Rev. B **78**, 075121 (2008)
27. K. Byczuk, M. Sekania, W. Hofstetter, A. Kampf, Phys. Rev. B **79**, R121103 (2009)
28. S.S. Kancharla, E. Dagotto, Phys. Rev. B **85**, 37006 (2009)
29. H. Chen, H. Zhao, H. Lin, C.Q. Wu, New J. Phys. **12**, 093021 (2010)
30. M. Sentef, J. Kunes, P. Werner, A.P. Kampf, Phys. Rev. B **80**, 155116 (2009)
31. A. Fuhrmann, D. Heilmann, H. Monien, Phys. Rev. B **73**, 245118 (2006)
32. H. Hafermann, M.I. Katsnelson, A.I. Lichtenstein, Eur. Phys. Lett. **85**, 37006 (2009)
33. G. Moeller, V. Dobrosavljević, A.E. Ruckenstein, Phys. Rev. B **59**, 6846 (1999)
34. S.S. Kancharla, S. Okamoto, Phys. Rev. B **75**, 193103 (2007)
35. K. Bouadim, G. Batrouni, F. Herbert, R. Scalettar, Phys. Rev. B **77**, 144527 (2008)
36. S. Hüfner, *Photoelectron Spectroscopy* (Berlin, Verlag, Springer, 1995)
37. F. Schuman, J. Kirschner, J. Berakdar, Phys. Rev. Lett. **95**, 117601 (2005)
38. F. Schumann, N. Fominykh, C. Winkler, J. Kirschner, J. Berakdar, Phys. Rev. B **77**, 235434 (2008)
39. R. Herrmann, S. Samarin, H. Schwabe, J. Kirschner, Phys. Rev. Lett **81**, 2148 (1998)
40. E. Weigold, M. Vos, *Many Particle Spectroscopy of Atoms, Molecules, Cluster and Surfaces*, edited by J. Berakdar, J. Kirschner (Kluwer Academic/Plenum Publishers, New York, 2001)
41. O. Artamonov, S. Samarin, J. Kirshner, J. Appl. Phys. A **65**, 535 (1997)
42. J. Berakdar, Phys. Rev. B **58**, 9808 (1998)
43. N. Fominykh, J. Henk, J. Berakdar, P. Bruno, Surf. Sci. **507**, 229 (2002)
44. N. Fominykh, J. Henk, J. Berakdar, P. Bruno, Phys. Rev. Lett. **89**, 086402 (2002)
45. N. Fominykh, J. Henk, J. Berakdar, P. Bruno, H. Gollisch, R. Feder, Solid State Commun. **113**, 666 (2000)
46. K. Kouzakov, J. Berakdar, J. Phys.: Condens. Matter **15**, L41 (2003)
47. B. Napitu, J. Berakdar, Phys. Rev. B **81**, 195108 (2010)
48. J. Hirsch, R. Fye, Phys. Rev. Lett. **56**, 2521 (1986)
49. M. Jarrell, J. Gubernatis, Phys. Rep. **269**, 133 (1996)